Eksploatacja i Niezawodnosc – Maintenance and Reliability
Volume 23 (2021), Issue 2
journal homepage: http://www.ein.org.pl
Article citation info:
Zhu Q, Sun W, Zhoua Y, Gao C. A tool wear condition monitoring approach for end milling based on numerical simulation. Eksploatacja i Niezawodnosc – Maintenance and Reliability 2021; 23 (2): 371–380, http://doi.org/10.17531/ein.2021.2.17.

A tool wear condition monitoring approach for end milling based on numerical simulation

Indexed by:
Web of Science Group

Qinsong Zhu[a], Weifang Sun[a], Yuqing Zhou[a,*], Chen Gao[b,*]

[a] College of Mechanical and Electrical Engineering, Wenzhou University, Wenzhou, China
[b] School of Mechatronics and Transportation, Jiaxing Nanyang Polytechnic Institute, Jiaxing, China

Highlights

- A numerical simulation model is proposed to overcome sample missing and insufficiency.
- Model parameters are optimized by orthogonal experiment and KL divergence.
- The optimized model provide effectively missing samples and expand sample size.
- Experimental results show the proposed method improves notably the performance of TCM.

Abstract

As an important research area of modern manufacturing, tool condition monitoring (TCM) has attracted much attention, especially artificial intelligence (AI)- based TCM method. However, the training samples obtained in practical experiments have the problem of sample missing and sample insufficiency. A numerical simulation- based TCM method is proposed to solve the above problem. First, a numerical model based on Johnson-Cook model is established, and the model parameters are optimized through orthogonal experiment technology, in which the KL divergence and cosine similarity are used as the evaluation indexes. Second, samples under various tool wear categories are obtained by the optimized numerical model above to provide missing samples not present in the practical experiments and expand sample size. The effectiveness of the proposed method is verified by its application in end milling TCM experiments. The results indicate the classification accuracies of four classifiers (SVM, RF, DT, and GRNN) can be improved significantly by the proposed TCM method.

Keywords

tool wear, sample missing, sample insufficiency, numerical simulation, cutting force.

1. Introduction

Computer numerical control (CNC) milling machines, which stable and efficient operation can produce huge economic value, are the most widely used automatic production equipment in modern manufacturing industry. The milling tool is the most critical and vulnerable part in the milling process, its wear state affect directly the surface quality of the machined parts and the normal operation of the machine tool [20, 21, 37]. Therefore, it is particularly important to develop an accurate tool condition monitoring (TCM) method.

The above-discussed issue has been addressed in the past few years by developing two general types of TCM methods, direct TCM method and indirect TCM method. The direct TCM method is often seldom adopted because it is greatly affected by the machining environment, such as light, cutting chips, and cutting fluid [49]. In contrast, the indirect TCM method employs certain artificial intelligence (AI) classifier to predict the wear state through collecting sensor signals associated with the tool wear state [33], such as cutting force [15, 50], vibration [6], acoustic emission (AE) [44], and motor current [47], sound [19, 46] signals. Recently, with the development of artificial intelligence (AI) algorithms, more and more scholars have applied AI algorithms in TCM, including support vector machine (SVM) [6,18], random forest (RF) [24, 32, 41], decision tree (DT) [3, 26], artificial neural network (ANN) [1, 9, 12, 22, 23, 28, 34]. However, while these AI methods have yielded encouraging achievements in TCM applications, achieving good wear state prediction performance using these methods relies heavily on large datasets of monitoring signals that are associated with all possible tool wear conditions for model training [14, 45], which is costly and time-consuming for machining processes under different cutting conditions. Although SVMs are suitable for model training with small datasets, they are invalid for sample missing as samples associated with some tool wear conditions are often missing due to the complex conditions encountered in the machining process.

Therefore, a low-cost and easy-to-implement method is needed to solve the problem of sample missing and sample insufficiency. In recent years, the numerical simulation technology was promoted by the improvement of computer technology, more and more researchers have begun to pay attention to this technology [16, 27, 40, 43]. For example, Xiang et al. [42] proposed a personalized diagnosis method of shaft based on numerical simulation, combined with wavelet packet transform (WPT) and SVM model to realize the diagnosis of different shaft faults. Gao et al. [7] solved the problem of missing and insufficient samples of bearing faults by combining finite element

(*) Corresponding author.
E-mail addresses: Q. Zhu - 1053876272@qq.com, W. Sun - vincent_suen@126.com, Y. Zhoua - zhouyq@wzu.edu.cn, C. Gao - gaochen_1993@163.com

simulation (FEM) and Generative adversarial networks (GANs), and provided complete training samples for AI models.

The metal cutting process can be understood as a process in which the tool and the workpiece move and collide with each other. The actual machining process can be simulated by establishing models and mathematical expressions. At present, there are a lot of commercial software (such as Deform, AdvantEdge, Abaqus.) in the market that encapsulate the above process in the software to bring convenience to users. The rich functions of these softwares provide the potentials to simulate physical signal corresponding to tool wear state, which can overcome the problem of sample missing and insufficient. Therefore, a novel tool wear condition monitoring method based on numerical simulation is proposed in this paper, and the remainder of this paper is organized as follows. Section 2 introduces the basic working principles of the proposed method, including numerical simulation based on Johnson-Cook (J-C) constitutive model, parameter optimization of the J-C model, and the framework of the proposed method. Experimental investigations with end milling TCM are given in Section 3. Section 4 analyzes the performance of the proposed method. Finally, conclusions are given in Section 5.

2. Proposed method

2.1. Numerical simulation based on J-C model

The essence of the cutting process is that the workpiece material from elastic deformation to the material yield point under the action of external forces, which causes the plastic deformation of workpiece and finally to the process of fracture. In this process, the tool contact and rub against with the workpiece surface and chips to produce wear, cutting force and heat will also be generated between the tool and workpiece. In cutting simulation, material constitutive models are employed to describe this complex process, and the J-C model is often used because it can describe the behavior of high temperature, high strain, and high strain rate in the cutting process. The formula of the J-C model is as follows [36]:

$$\sigma = \left(A + B\varepsilon^{\mathrm{n}}\right)\left(1 + C\ln\left(\frac{\varepsilon'}{\varepsilon_0'}\right)\right)\left(1 - \left(\frac{T - T_0}{T_{melt} - T_0}\right)^{\mathrm{m}}\right) \tag{1}$$

where A (MPa) is the initial yield stress, B (MPa) is the strain hardening coefficient, ε is the the plastic strain, n is the stain hardening exponent, C is the strain rate sensitivity coefficient, ε' and ε_0' are the plastic strain rate (s^{-1}) and reference plastic strain rate (s^{-1}), respectively, T is the deformation temperature of the workpiece (°C), T_0 is room temperature (20°C), T_{melt} is the melting temperature of the material (°C), and m is the temperature softening exponent [13]. the three individual terms separately enclosed within parentheses on the right side of formula (1), respectively, represent the strain strengthening effect of the material, the relationship between σ and the natural logarithm of the relative strain rate, and the exponential relationship between σ and temperature.

Because of the rich material library and the specialized cutting module in software DEFORM, it has attracted the attention of many researchers to the software. Shao et al. [35] adopted DEFORM to study the thermodynamic constitutive equation of Ti-6Al-4V and predicted the tool wear depth. Klocke et al. [17] utilized DEFORM to inverse the constitutive equations and damage criteria of AISI 1045 and Inconel 718, and verified the effectiveness of the method by comparing simulation results with experimental results. Thus, the software DEFORM is used in this paper to simulate the end milling process and obtain the missing wear samples.

2.2. Parameter optimization

The benchmark value of five parameters, A, B, n, C, m, in the J-C model with certain workpiece material can be obtained from split Hopkinson pressure bar (SHPB) tests and static tensile tests [2,30]. For example, the benchmark value of the five parameters are shown in Table 1 when the workpiece material is AISI 1045. However, these values of model parameters may not conform the practical cutting process because of different cutting environment and other various factors, so it is necessary to optimize these model parameters [4]. Considering the cost and time of experiments, orthogonal experiment is adopted to select the best parameter combination.

Table 1. Material parameters in J-C model of workpiece material AISI 1045

	A (MPa)	B (MPa)	C	n	m	T_{room} (°C)	T_{melt} (°C)
Value	553.1	600.8	0.0134	0.23	1	20	1460

For the metrics, Kullback-Leibler (KL) [5,8] divergence and cosine similarity are used as the evaluation indexes of the orthogonal experiment. The KL divergence measures the difference in probability distribution of two groups of signal, and the closer the value of KL is to 0, the more similar the two groups of signal are. The formula of KL divergence is as follows [5]:

$$D_{KL}[p \,\|\, q] = \int_{-\infty}^{+\infty} p(X)\log\frac{p(X)}{q(Y)}dx \tag{2}$$

where $p(X)$ and $q(Y)$ represent the probability density of two groups of signal, respectively. The cosine similarity evaluates the similarity of two groups of signal through calculating their cosine value, and the calculation formula is as follows:

$$\cos(\theta) = \frac{X \bullet Y}{\|X\| \times \|Y\|} = \frac{\sum_{\mathrm{i}=1}^{\mathrm{n}} X_i \times Y_i}{\sqrt{\sum_{\mathrm{i}=1}^{\mathrm{n}} (X_i)^2} \times \sqrt{\sum_{\mathrm{i}=1}^{\mathrm{n}} (Y_i)^2}} \tag{3}$$

The closer the value of $\cos(\theta)$ is to 1, the more similar the two groups of signal are. In actual engineering, it is generally considered that $\cos(\theta) > 0.6$ meets the requirements [29].

2.3. Framework of the proposed method

In this paper, a new TCM method based on numerical simulation is proposed to compensate missing samples and expand sample size. The framework of the proposed method is show in Figure 1, and the three steps of the proposed TCM are outlined in detail as follows.

Step 1: Conduct a limited number of milling TCM experiments to obtain measured cutting force signal samples, and obtain the best parameter combination of the J-C model under normal wear state of tool .

First, cutting force signal data is obtained in the milling experiments under several selected tool wear conditions by means of a three-component dynamometer. Second, the numerical model based on the J-C model is built in DEFORM, and the best parameter combination is selected by the orthogonal experiment with the comparative analysis of the simulation signal and the experimental signal under the normal tool condition, in which the criteria is minimize KL divergence satisfying the $\cos(\theta) > 0.6$.

Step2: Simulate missing sample and obtain complete wear training samples.

Table 2. Feature parameters and the calculation formulas

Domain	Feature parameter	Formula	Remarks
Time domain	Average	$T_1 = \sum_{i=1}^{n} x_i / n$	x_i (i = 1, 2, ..., n) represents the original collected signal sequence.
	Root mean square	$T_2 = \sqrt{\sum_{i=1}^{n} x_i^2 / n}$	
	Standard deviation	$T_3 = \frac{1}{n-1}\sqrt{\sum_{i=1}^{n}(x_i - T_{avg})^2}$	
	Crest factor	$T_4 = \max\{\lvert x_i \rvert\} / T_{rms}$	
	Shape factor	$T_5 = T_{rms} / T_{avg}$	
	Skewness	$T_6 = (\sum_{i=1}^{n}(x_i - T_{avg})^3) \Big/ (n \cdot T_{sd}^3)$	
	Kurtosis	$T_7 = (\sum_{i=1}^{n}(x_i - T_{avg})^4) \Big/ (n \cdot T_{sd}^4) - 3$	
	Waveform	$T_8 = n \cdot T_{rms} \Big/ (\sum_{i=1}^{n} \lvert x_i \rvert)$	
	Margin factor	$T_9 = n^2 \cdot \max\{\lvert x_i \rvert\} \Big/ (\sum_{i=1}^{n} \lvert x_i \rvert)^2$	
Frequency domain	Mean of power spectrum	$F_1 = \sum_{j=1}^{n} P_j / n$	f_i represents the frequency corresponding to x_i; P_i represents the power spectrum of f_i.
	Root mean square of power spectrum	$F_2 = \sqrt{\sum_{j=1}^{n} P_j^2 / n}$	
	Crest factor of power spectrum	$F_3 = \max\{P_i\} \Big/ \sqrt{\sum_{j=1}^{n} P_j^2 / n}$	
	Modified equivalent bandwidth	$F_4 = \sqrt{(\sum_{j=1}^{n}(f_j - \bar{f})^2 P_j) \Big/ (\sum_{j=1}^{n} P_j)}$	
	High-low ratio of power spectrum	$F_5 = (\sum_{j=n/4}^{n/2} P_j) \Big/ (\sum_{j=1}^{n/4} P_j)$	
	Stabilization ratio	$F_6 = (\sum_{j=1}^{n} f_j^2 P_j) \Big/ (\sqrt{\sum_{j=1}^{n} P_j}\sqrt{\sum_{j=1}^{n} f_j^4 P_j})$	
	Skewness of bandpower	$F_7 = (\sum_{j=1}^{n}(P_j - F_{mps})^3) \Big/ (\sum_{j=1}^{n}(P_j - F_{mps})^2)^{\frac{3}{4}}$	
	Kurtosis of bandpower	$F_8 = n(\sum_{j=1}^{n}(P_j - F_{mps})^4) \Big/ (\sum_{j=1}^{n}(P_j - F_{mps})^2)$	
Time-frequency domain	Wavelet energy coefficient	$E_j = \frac{1}{n}\sum_{k=1}^{n}(d_{j,k})^2 = \frac{1}{n}\sum_{k=1}^{n}(\int w_{j,k}(t)x(t)dt)^2$	

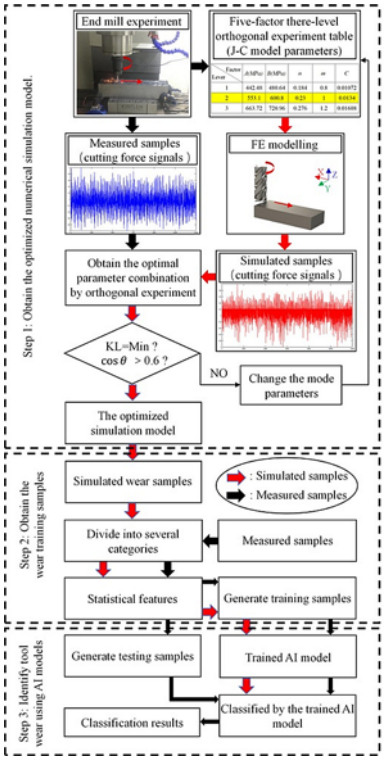

Fig. 1. Framework of the proposed TCM method

Missing tool wear categories can be defined from the experimental results, that is, these categories not occurred in experiments are missing tool wear categories. These missing tool wear categories can be simulated based on the optimal numerical model above, and the corresponding cutting force signal could be obtained. After supplementing missing samples, several feature parameters (shown in Table 2) of time, frequency, and time- frequency domains (wavelet energy coefficient) for each sample are extracted to form a feature parameter set [7, 25, 37, 48]. Here, the time-frequency domain parameter was obtained using the three-layer wavelet packet transform (WPT) with the Daubechies 2 (db2) wavelet basis function.

Step 3: Identify tool wear condition through AI classifiers.

The training set consists of simulated samples and measured samples, and inputs to train certain AI model. The trained AI model can be employed to identify unknown wear condition of tools.

3. Experimental investigations

3.1. Description of experiments

The experimental setup for the end milling TCM experiments under various operating conditions is illustrated in Figure 2. The experimental platform was built on a DMTG VDL850A vertical machining center as shown in Figure 2(a). The tools used in the experiments were uncoated three-flute tungsten steel end milling cutters (Φ 10 mm), and the workpiece material was AISI 1045 steel with dimensions of 300 mm × 100 mm × 80 mm. A three-component dynamometer (Kistler 9139AA) was mounted between the workpiece and the machine table to measure the cutting forces in the form of charges (shown in Figure 2(b)). The cutting force signal (Axial force, radial force and tangential force) was collected by a charge amplifier (Kistler 5073 A4) and a data acquisition instrument (Kistler 5697 A1) with a sampling frequency of 12 kHz (shown in Figure 2(c)). As shown in Figure 2(d), the flute wear of each cutting tool was measured after each machining stage using a GP-300C optical microscope, which represented individual milling stages. It is noteworthy that we found the influence of the length of rake face wear (KB) on the surface roughness of the workpiece after

a)

b)

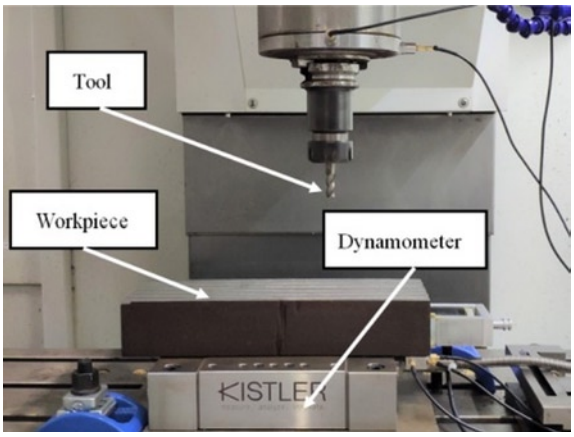

c)

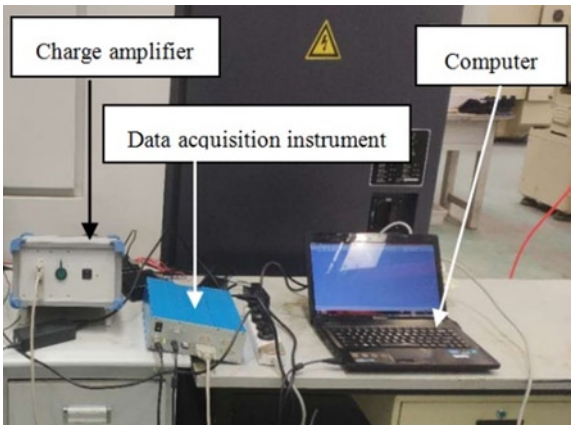

d)

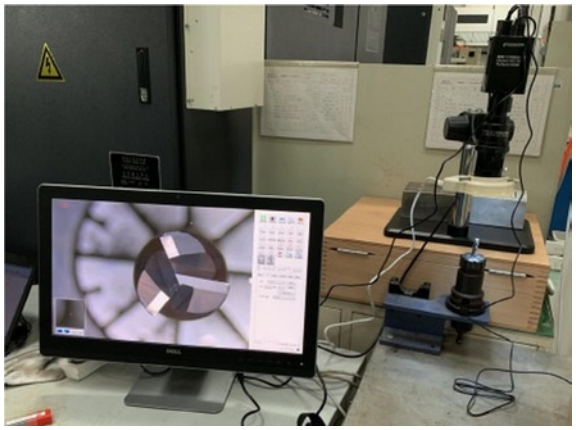

Fig. 2. Experimental end milling TCM setup [25]: a) vertical machining center, b) end milling experimental platform, c) data acquisition instrument, d) tool microscope

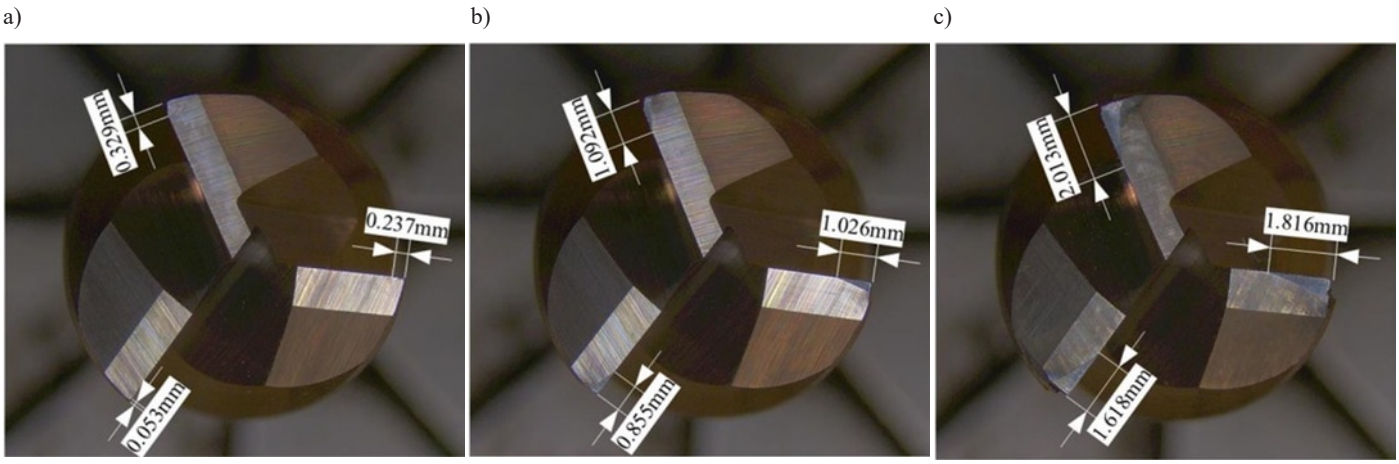

Fig. 3. Tool images indicative of different length of rake face wear (KB) values [46]: a) first milling stage, b) fifth milling stage, c) tenth milling stage

Table 3. Experimental cutting parameters

Case	Spindle Speed (rpm)	Depth of Cut (mm)	Feed Rate (mm/min)
1	2300	0.4	400
2	2300	0.6	500
3	2400	0.4	450
4	2400	0.5	500
5	2500	0.5	400
6	2500	0.6	450
7	2300	0.4	500
8	2300	0.6	400

Table 4. Tool wear classifications of the eight milling tools

Category / Case	1-st [0, 0.3)	2-nd [0.3, 0.6)	3-rd [0.6, 0.9)	4-th [0.9, 1.2)	5-th [1.2, 1.5)	6-th [1.5, 1.8)	7-th ≥1.8	Sample number
1	—	2	2	2	—	2	2	10
2	1	1	1	3	1	3	—	10
3	—	2	1	3	1	2	1	10
4	—	2	2	2	1	3	—	10
5	1	2	2	3	2	—	—	10
6	—	2	2	2	1	1	2	10
7	2	2	3	1	2	—	—	10
8	1	1	2	1	1	4	—	10

milling was greater than that of flank wear (VB) and the depth of rake face wear (KT) [47]. Therefore, KB was employed as the tool wear criterion in the experiments, and the tool wear value after each cutting stage was defined as the maximum KB value of the three teeth. Figure 3 illustrates the progression of tool wear after finishing a single workpiece surface 1, 5, and 10 times (i.e., 1, 5, and 10 milling stages).

The experimental measurements employed eight operational conditions comprising random combinations of three operational parameters: spindle speed, depth of cut, and feed rate. The operational parameters employed in the experiments are listed in Table 3. Each case began with a new tool under the eight operational conditions and ran 10 milling stages, and the largest tool wear value obtained after completing those milling stages in all eight conditions was 2.054 mm. Therefore, the milling tool wear condition was divided into 7 categories according to tool wear intervals of 0.3 mm, and the numbers of samples observed for all conditions in all categories are listed in Table 4. It can be found in Table 4 that samples indicative of individual tool wear categories were not always available under all cutting conditions. These represent missing samples.

3.2. Numerical simulation of end milling process

First, simulation modeling was carried out according to the dimensions of workpiece and milling tool in the experiment, then the models are imported into DEFORM for processing. Second, the general preprocessing module of DEFORM was selected in the main interface, and the unit standard was set as SI. The workpiece was set as a plastic body and the material was set as AISI 1045. The tool was set as a rigid body and the material was set as tungsten carbide steel. The mechanical characteristics of these materials were imported from the rich material library in DEFORM. Then, the J-C model was selected for the workpiece material model, and the benchmark parameters of J-C model are shown in Table 1. The number of meshes for the workpiece and tool were 40,000 and 10,000, respectively. Considering the efficiency of remeshing during calculation to reduce the time of the entire milling simulation calculation, the mesh type in the model was set to a tetrahedral mesh. And the mesh size could be set to 1/3 of feed rate per spindle speed [31,39], thus according to Table 3 the mesh size could be calculated to 0.053 mm (400/2500/3 = 0.053mm). Reasonable simulation speed and accuracy was ensured by applying local refinement to the machined surface, and the refinement ratio was 0.01. After inspection, the maximum mesh size of the workpiece and the tool is less than 1/5 of the feed. Figure 4(a), (b) and (c) show the milling tool model, meshing refinement, and simulation running in DEFORM, respectively.

For boundary conditions, the bottom of the workpiece was fixed in the three directions (X, Y, and Z), the entire surface of the workpiece and tool were selected for heat exchange with the environment, the three operational parameters (spindle speed, depth of cut, and feed rate) of cutting processing were set in according to actual conditions in Table 3. The number of simulation steps was set 24000, and the sampling interval was 8.33×10^{-5} *s* and the sampling time was 1 s. In modeling the tool/workpiece contact, the friction coefficient between the tool and the workpiece was 0.6 [10], and the thermal conductivity was 45 $W \cdot m^{-1} \cdot C^{-1}$ [11]. Finally, after simulation, the cutting force data was exported and saved in the post-processing.

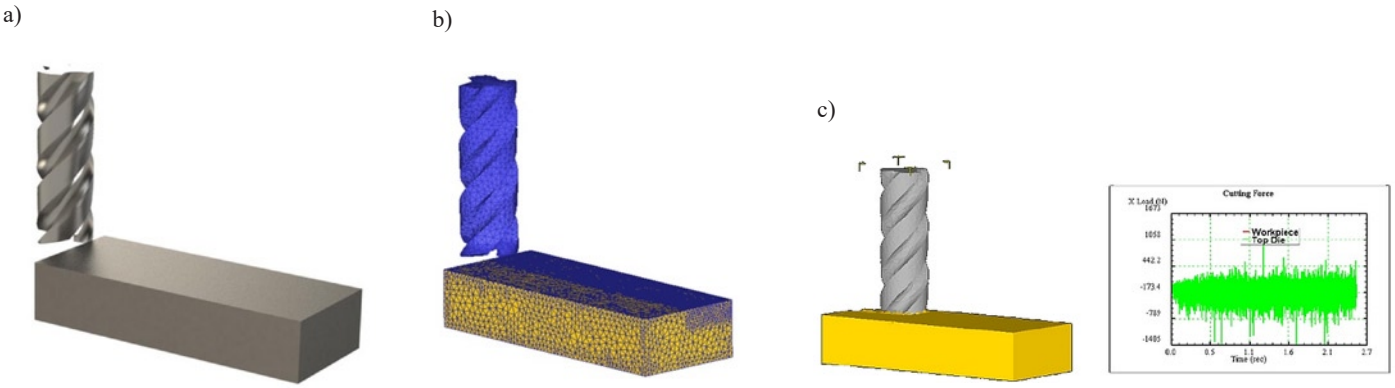

Fig. 4. Simulation of end milling process: a) milling tool model, b) meshing and refinement, c) simulation running

Table 5. Factor level table

Level	A	B	n	m	C
1	442.48	480.64	0.184	0.8	0.01072
2	553.1	600.8	0.23	1.0	0.0134
3	663.72	720.96	0.276	1.2	0.01608

used in the orthogonal experiment were 2500 rpm, 0.6 mm, and 450 mm/min, respectively. Therefore, the experimental data of the same parameters were selected to calculate the KL divergence and cosine similarity, and the comparison data is taken one second (12,000 data points) after the milling tool completely entered the workpiece. The KL divergence and cosine similarity results of the 18 cutting tests are shown in Table 6.

Table 6. Orthogonal experiments of the J-C model parameters

No.	A	B	n	m	C	Average KL	Average Cos(θ)
1	1	1	1	1	1	2.9240	0.6991
2	1	2	2	2	2	2.8078	0.7233
3	1	3	3	3	3	3.0946	0.6942
4	2	1	1	2	2	2.6832	0.7299
5	2	2	2	3	3	2.9804	0.7236
6	2	3	3	1	1	3.0403	0.7211
7	3	1	2	1	3	2.8987	0.6954
8	3	2	3	2	1	2.8236	0.7013
9	3	3	1	3	2	3.1400	0.7136
10	1	1	3	3	2	3.1034	0.7165
11	1	2	1	1	3	3.0441	0.6957
12	1	3	2	2	1	3.0547	0.7229
13	2	1	3	1	1	2.8985	0.7366
14	2	2	1	2	2	2.9507	0.7101
15	2	3	2	3	3	2.8640	0.7099
16	3	1	2	2	3	2.9140	0.6970
17	3	2	3	3	1	2.8981	0.6996
18	3	3	1	1	2	2.9098	0.6942
Average KL of the 1-st level	3.0048	2.9036	2.9420	2.9526	2.9399	——	——
Average KL of the 2-nd level	2.9029	2.9175	2.9199	2.8723	2.9325	——	——
Average KL of the 3-rd level	2.9307	3.0172	2.9764	3.0134	2.9660	——	——
Benchmark	2	2	2	2	2	2.7516	0.7196
The optimal	2	1	2	2	2	2.6035	0.7389

3.3. Parameter optimization by orthogonal experiments

In this section,three levels of each parameter in Table 1 were set as 80%, 100% and 120% of the benchmark value (shown in Table 5), and an orthogonal table of five factors and three levels (L_{18} (5^3)) was employed to conduct the orthogonal experiments, as shown in Table 6. The operational parameters (speed, depth of cut, and feed rate)

The KL divergence and cosine similarity results of each orthogonal experiment case were presented in Table 6, in which the values of KL divergence and cosine similarity are the average of three directions (X, Y and Z). By main effect analysis, the best parameter combination is A(2) B(1) n(2) m(2) C(2), as shown in Table 6, the corresponding average KL divergence is 2.6035, which is smaller than the other com-

binations, and the average cosine similarity values (= 0.7389) greater than 0.6. The simulated and measured time series data corresponding to the best parameter combination under normal tool condition are presented in Figure 5 in the *X*, *Y*, and *Z* directions. It can be seen that the simulated signals differ slightly from the measured signals.

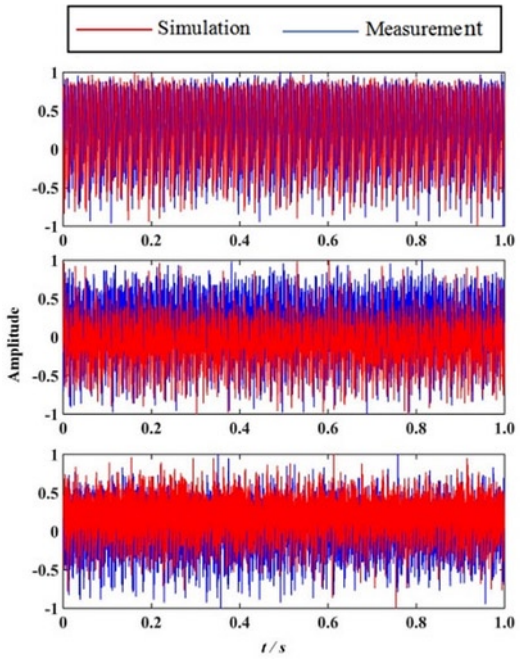

Fig. 5. The time-domain comparison between measured and simulation signals

4. Result analysis

4.1. Simulation signal verification

The validity of the simulated samples were tested by comparing 1.0 s (i.e., 12,000 sampling points) of the simulated and measured cutting force signals obtained for operational condition 6 under different tool wear categories. Figures 6-8 show the time series data and the corresponding frequency spectra of the simulated and measured signal in the *X*, *Y*, and *Z* directions under the 2-nd, 4-th and 10-th tool wear categories. It can be seen that, under these tool wear categories, the simulated signals differ slightly from the measured signals in terms of the amplitudes of the peaks in the frequency domain, while the frequency peak positions agree well.

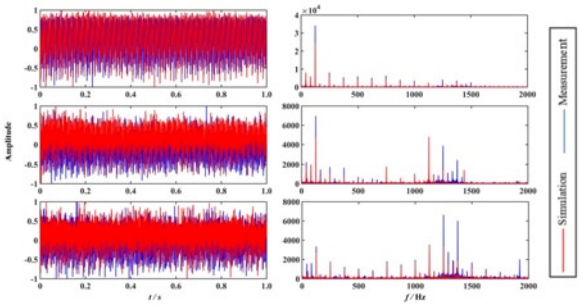

Fig. 6. Comparison of the simulated and measured cutting force signals under the 2-nd tool wear category

4.2. Sample augmentation

As shown in Figure 6, different tool wear states were simulated based on the optimal numerical simulation model according to the tool wear lengths and wear shapes obtained during the experiments, and the linear interpolation method was applied to achieve KB values less than the threshold for missing categories according to the observed tool wear value trends. Three examples of wear categories

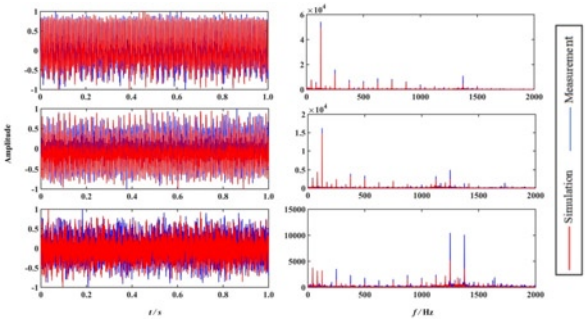

Fig. 7. Comparison of the simulated and measured cutting force signals under the 4-th tool wear category

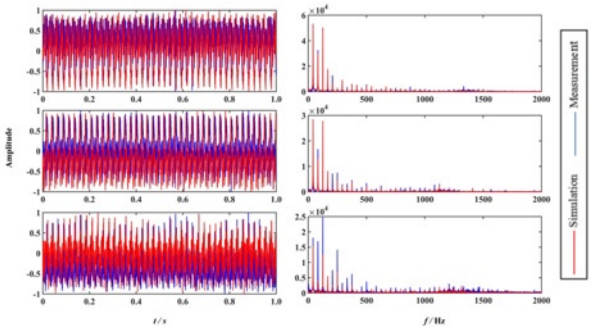

Fig. 8. Comparison of the simulated and measured cutting force signals under the 10-th tool wear category

added based on the FEM model are presented in Fig. 6 for operational condition 6.

According to Table 4, the 1-st and 7-th wear categories were generally missing under the operational conditions considered. Therefore, we consider missing samples only for the 7-th category here owing to article length limitations. Cases 2, 4, 5, 7, and 8 were employed as the training dataset because all of these are missing the 7-th wear category, and the remaining three cases 1, 3, and 6, which contain the 7-th category but not the 1-st category, were employed as the testing dataset. Then, 12,000 data points (1 s) were selected for the simulated and measured samples of each category, which are evenly divided into 20 groups. The optimal numerical simulation model model is employed to simulate the testing cases (Cases 1, 3, and 6) to increase the number of samples in the training dataset. Each simulated case contains 12 different tool KB samples involving all wear categories, and the sample sizes of the measured and simulated training sets were 900 (45×20) and 560 (28×20) not including the 1-st category, respectively. Accordingly, we employed three separate datasets to train the AI classifiers, which included the measurement dataset composed of only measured samples, the simulation dataset composed of only simulated samples, and the measurement + simulation dataset composed of measured and simulated samples, with a total of 1460 (900+560) samples.

4.3. Classification result and analysis

These feature parameters listed in Table 2 were calculated for the individual samples in the training and testing datasets, and employed as the input parameters for training and testing classifiers. Four common algorithms, SVM, RF, DT, and a generalized regression neural network (GRNN), were adopted to verify the generalized ability of the proposed method. Here, the SVM classifier selects the radial basis kernel function, and the penalty factor and kernel function radius are set to 3 and 1, respectively. The RF classifier was executed with the Randomforest-matlab open source toolbox developed by Abhishek Jaiantilal (https://github.com/ajaiantilal/ randomforest-matlab), and the number of decision trees was set to 500. The DT classifier was used the toolbox function ClassificationTree.fit in MATLAB R2016, and the parameters of 'name' and 'value' were selected as 'model' and

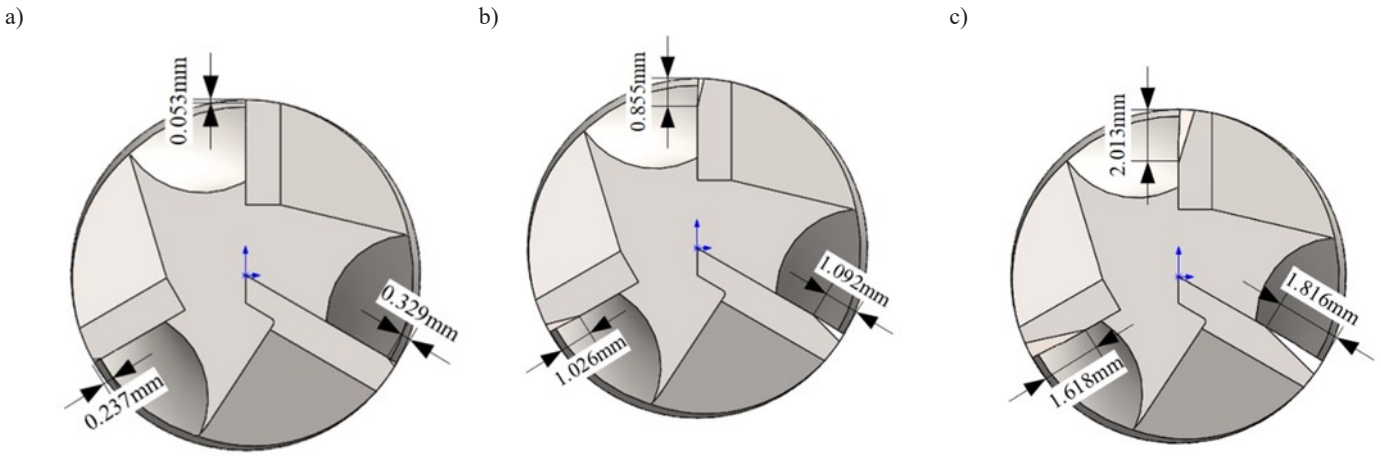

Fig. 9. Artificially added wear categories obtained from the FEM model: a) second category, b) fourth category, c) seventh category

Table 7. Classification Accuracy of four classifiers with different samples

Training set	Measure-ment	Simulation	Measurement + Simu-lation
SVM	68.67%	85.67%	91.33%
RF	73.50%	90.17%	93.83%
DT	70.00%	56.67%	90.00%
GRNN	54.67%	80.00%	83.00%
Average accuracy	66.71%	78.13%	89.54%

tion dataset is greater than that based on the measurement dataset by 11.42%, although the sample size of the simulation datset is less than that of the measurement dataset. There are two reasons for this result, one is the simulation dataset makes up missing categories not occurred in experiments, the other is the cutting conditions corresponding to the simulation dataset are consistent with that to the testing dataset. In addition, the average classification accuracy obtained by the classifiers based on the measurement + simulation dataset is greater than that based on the measurement dataset by 22.83%, and the classification accuracies obtained by the SVM, RF, and DT classifiers based on the measurement + simulation dataset are above 90%. Therefore, it can be

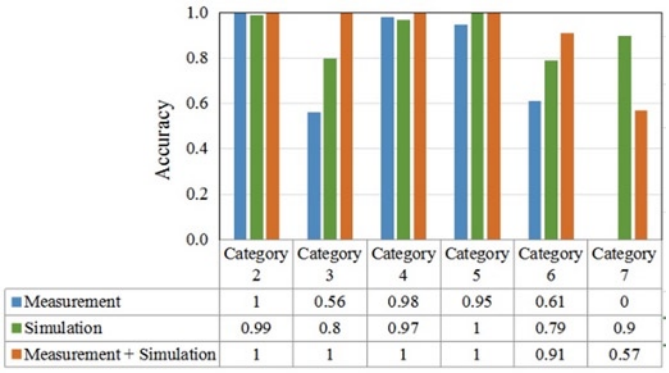

Fig. 10. Classification accuracy of each wear category using the SVM with three training datasets

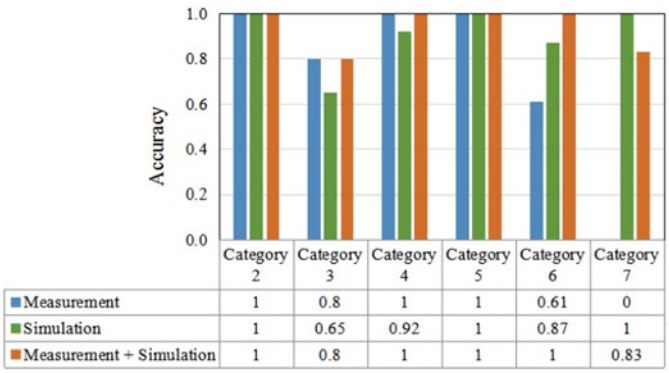

Fig. 11. Classification accuracy of each wear category using the RF with three training datasets

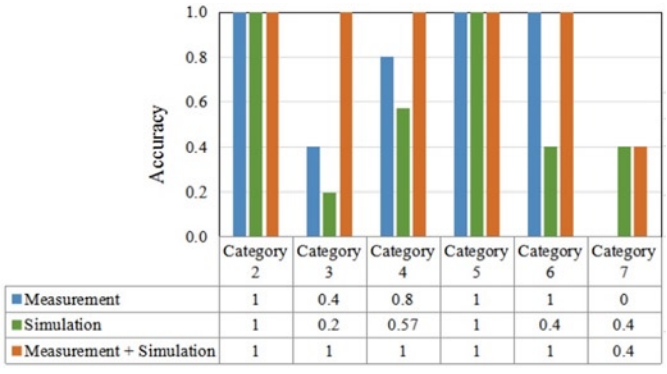

Fig. 12. Classification accuracy of each wear category using the DT with three training datasets

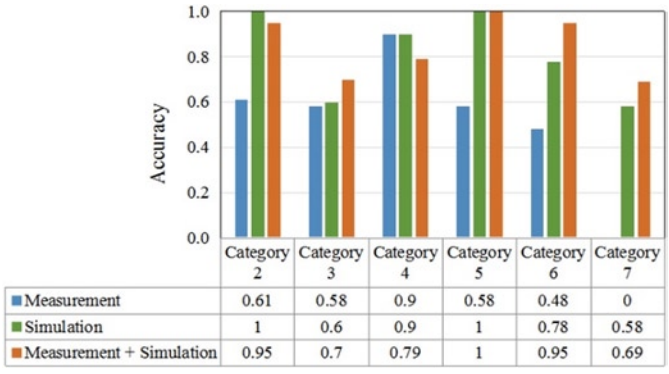

Fig. 13. Classification accuracy of each wear category using the GRNN with three training datasets.

'graph', respectively. The value of SPREAD in the GRNN classifier was set to 0.1.

Table 7 shows the classification accuracies of four classifiers with the testing dataset. It can be found from Table 7, that the average classification accuracy obtained by the classifiers based on the simula-

considered that the proposed TCM method can improves significantly the classification accuracies of many classifiers.

The classification accuracy of each wear category obtained using the four classifiers trained using the three different training datasets are presented in Figures 10-13, respectively. We note from the figures

that the classification accuracy of the four classifiers trained with the measurement dataset is not high for most of the wear categories. In contrast, the classification accuracy of the four classifiers trained with the simulation dataset and the measurement + simulation dataset are generally much greater (except for wear category 3 in RF and wear category 4 in GRNN, which are lower).

5. Conclusion

This paper proposed a feasible TCM method for obtaining various samples of tool wear condition by numerical simulation based on J-C model to overcome the problem of sample missing and sample insufficiency in real experiments. First, a numerical model based on Johnson-Cook model is established, and the model parameters are optimized through orthogonal experiment technology with the practical experiments, in which the Kullback- Leibler divergence and cosine similarity are used as the evaluation indexes. Second, samples under various tool wear categories are obtained by the optimized numerical model above to provide missing samples not present in the practical experiments and expand sample size. The effectiveness of the proposed method is verified by its application in end milling TCM experiments. The results indicate the classification accuracies of four classifiers (SVM, RF, DT, and GRNN) can be improved significantly by the proposed TCM method, and we believe that the proposed method has similar effects on other AI classifiers. In addition, although this study is about tool wear condition monitoring approach for end milling, the proposed method is also applicable to other machining process.

Acknowledgements

This work was supported in part by the National Natural Science Foundation of China under Grant 51405346, in part by the Zhejiang Provincial Natural Science Foundation of China under Grant LY17E050005, and in part by the Wenzhou Key Innovation Project for Science and Technology of China under Grant ZD2019042.

References

1. Chen QP, Xie QS, Yuan QN, Huang HS, Li YT. Research on a real-time monitoring method for the wear state of a tool based on a convolutional bidirectional LSTM model. Symmetry-Basel 2019; 11(10) 1233, https://doi.org/10.3390/sym11101233.
2. Duan CZ, Yu HY, Cai YJ, Li YY. Finite Element Simulation and Experiment of Chip Formation during High Speed Cutting of Hardened Steel. Applied Mechanics and Materials 2010; 29-32: 1838-1843, https://doi.org/10.4028/www.scientific.net/AMM.29-32.1838.
3. Duan R, Lin Y, Zeng Y. Fault diagnosis for complex systems based on reliability analysis and sensors data considering epistemic uncertainty. Eksploatacja i Niezawodnosc - Maintenance and Reliability 2018, 20(4): 558-566, https://doi.org/10.17531/ein.2018.4.7
4. Ducobu F, Rivière-Lorphèvre E, Filippi E. On the importance of the choice of the parameters of the Johnson-Cook constitutive model and their influence on the results of a Ti6Al4V orthogonal cutting model. International Journal of Mechanical Sciences 2017; 122: 143-155, https://doi.org/10.1016/j.ijmecsci.2017.01.004.
5. Erven T, Harremoës P. Rényi divergence and Kullback-Leibler divergence. IEEE Transactions on Information Theory 2014; 60(7): 3797-3820, https://doi.org/10.1109/TIT.2014.2320500.
6. Gao C, Xue W, Ren Y, Zhou YQ. Numerical control machine tool fault diagnosis using hybrid stationary subspace analysis and least squares support vector machine with a single sensor. Applied Sciences 2017; 7(4) 346, https://doi.org/10.3390/app7040346.
7. Gao Y, Liu XY, Xiang JW. FEM simulation- based generative adversarial networks to detect bearing faults. IEEE Transactions on Industrial Informatics 2020; 16(7): 4961-4971, https://doi.org/10.1109/TII. 2020.2968370.
8. Gkdere G, Mehmet G. New reliability score for component strength using kullback-leibler divergence. Eksploatacja i Niezawodnosc - Maintenance and Reliability 2016; 18(3): 367-372, https://doi.org/ 10.17531/ein.2016.3.7.
9. Huang ZW, Zhu JM, Lei JT, Li XR, Tian FQ. Tool wear predicting based on multi-domain feature fusion by deep convolutional neural network in milling operations. Journal of Intelligent Manufacturing 2020; 31(4): 953-966, https://doi.org/10.1007/s10845-019-01488-7.
10. Iqbal S, Mativenga PT, Sheikh MA. Characterization of machining of AISI 1045 steel over a wide range of cutting speeds. Part 1: investigation of contact phenomena. Proceedings of the Institution of Mechanical Engineers Part B Journal of Engineering Manufacture 2007; 221(5): 909-916, https://doi.org/10.1243/ 09544054JEM796.
11. Iqbal S, Mativenga PT, Sheikh MA. Characterization of machining of AISI 1045 steel over a wide range of cutting speeds. Part 2: Evaluation of flow stress models and interface friction distribution schemes. Proceedings of the Institution of Mechanical Engineers Part B Journal of Engineering Manufacture 2007; 221(5): 917-926, https://doi.org/10.1243/09544054JEM797.
12. Jasiulewicz-Kaczmarek M, Antosz K, Żywica P, Mazurkiewicz D, Sun B, Ren Y. Framework of machine criticality assessment with criteria interactions. Eksploatacja i Niezawodnosc - Maintenance and Reliability 2021; 23(2): 207-220, https://doi.org/10.17531/ein.2021.2.1.
13. Javidikia M, Sadeghifar M, Songmene V, Jahazi M. On the impacts of tool geometry and cutting conditions in straight turning of aluminum alloys 6061-T6: an experimentally validated numerical study. International Journal of Advanced Manufacturing Technology 2020; 106(9-10): 4547-4565, https://doi.org/ 10.1007/s00170-020-04945-3.
14. Karabacak YE, Ozmen NG, Gumusel L. Worm gear condition monitoring and fault detection from thermal images via deep learning method. Eksploatacja i Niezawodnosc - Maintenance and Reliability 2020; 22(3): 544-556, https://doi.org/10.17531/ein.2020.3.18.
15. Karandikar J, Mcleay T, Turner S, Schmitz T. Tool wear monitoring using naïve bayes classifiers. The International Journal of Advanced Manufacturing Technology 2015; 77(9-12): 1613-1626, https://doi.org/ 10.1007/s00170-014-6560-6.
16. Karwat B, Rubacha P, Stanczyk E. Simulational and experimental determination of the exploitation parameters of a screw conveyor. Eksploatacja i Niezawodnosc - Maintenance and Reliability 22(4): 741-747, https://doi.org/10.17531/ein.2020.4.18.
17. Klocke F, Lung D, Buchkremer S. Inverse identification of the constitutive equation of Inconel 718 and AISI 1045 from FE machining simulations. Procedia CIRP 2013; 8: 212-217, https://doi.org/10.1016/j. procir.2013.06.091.
18. Kong D, Chen Y, Li N, Duan C, Lu L, Chen D. Tool wear estimation in end milling of titanium alloy using npe and a novel woa-svm model. IEEE Transactions on Instrumentation and Measurement 2020; 69(7): 5219-5232, https://doi.org/10.1109/TIM.2019.2952476.
19. Kothuru A, Nooka SP, Liu R. Application of audible sound signals for tool wear monitoring using machine learning techniques in end milling. The International Journal of Advanced Manufacturing Technology 2018; 95(9-12): 3797-3808, https://doi.org/10.1007/s00170-017-1460-1.
20. Kozłowski E, Mazurkiewicz D, Zabinski T, Prucnal S, Sep J. Assessment model of cutting tool condition for real-time supervision system. Eksploatacja i Niezawodnosc - Maintenance and Reliability 2019; 21(4): 679-685, https://doi.org/10.17531/ein.2019.4.18.
21. Kozłowski E, Mazurkiewicz D, Żabiński T, Prucnal S, Sęp J. Machining sensor data management for operation-level predictive model.

Expert Systems with Applications 2020; 159: 1-22, https://doi.org/ 10.1016/j.eswa.2020.113600.
22. Kumar A, Kumar R. Adaptive artificial intelligence for automatic identification of defect in the angular contact bearing. Neural Computing and Applications 2018; 29: 277-287, https://doi.org/10.1007/s00521-017 -3123-4.
23. Kumar A, Kumar R. Least Square Fitting for Adaptive Wavelet Generation and Automatic Prediction of Defect Size in the Bearing Using Levenberg-Marquardt Backpropagation. Journal of Nondestructive Evaluation 2017; 36, 7, https://doi.org/10.1007/s10921-016-0385-1.
24. Küppers F, Albers J, Haselhoff A. Random Forest on an Embedded Device for Real-time Machine State Classification. 2019 European Signal Processing Conference (EUSIPCO), A Coruna, Spain, https://doi.org/10.23919/EUSIPCO.2019.8902993.
25. Lei Z, Zhou YQ, Sun BT, Sun WF. An intrinsic timescale decomposition-based kernel extreme learning machine method to detect tool wear conditions in the milling process. The International Journal of Advanced Manufacturing Technology 2020; 106(3-4): 1203-1212, https://doi.org/10.1007/s00170-019- 04689-9.
26. Li GF, Wang YB, He JL, Hao QB, Yang HJ, Wei JF. Tool wear state recognition based on gradient boosting decision tree and hybrid classification RBM. The International Journal of Advanced Manufacturing Technology 2020; 110: 511-522, https://doi.org/10.1007/s00170-020-05890-x.
27. Liu D, Wang S, Tomovic M. Degradation modeling method for rotary lip seal based on failure mechanism analysis and stochastic process. Eksploatacja i Niezawodnosc - Maintenance and Reliability 2020; 22(3): 381-390, https://doi.org/10.17531/ein.2020.3.1
28. Liu H, Liu ZY, Jia WQ, Lin XK, Zhang S. A novel transformer-based neural network model for tool wear estimation. Measurement Science and Technology 2020; 31(6) 065106, https://doi.org/10.1088/1361- 6501/ab7282.
29. Liu XY, Huang HZ, Xiang JW. A personalized diagnosis method to detect faults in gears using numerical simulation and extreme learning machine. Knowledge-Based Systems 2020; 105653, https://doi.org/10.1016/j.knosys.2020.105653.
30. Liu ZQ, Wu JH, Shi ZY, Zhao PF. State-of-the-art of Constitutive Equations in Metal Cutting Operations. Tool Engineering 2008; 42(3): 3-10 (in Chinese).
31. Padma RB, Kumara SM. Finite Element Simulation of a Friction Drilling process using Deform-3D. International Journal of Engineering Research and Applications 2012; 2(6): 716-721.
32. Pawełczyk M, Fulara S, Sepe M, Luca AD, Badora M. Industrial gas turbine operating parameters monitoring and data-driven prediction. Eksploatacja i Niezawodnosc - Maintenance and Reliability 2020; 22(3):391-399. https://doi.org/10.17531/ein.2020.3.2
33. Serin GB, Sener AM, Ozbayoglu HO. Review of tool condition monitoring in machining and opportunities for deep learning. International Journal of Advanced Manufacturing Technology 2020; 109(2): 953-974. https://doi.org/10.1007/s00170-020-05449-w.
34. Shankar S, Mohanraj T, Rajasekar R. Prediction of cutting tool wear during milling process using artificial intelligence techniques. International Journal of Computer Integrated Manufacturing 2019; 32(2): 174-182, https://doi.org/10.1080/0951192X.2018.1550681.
35. Shao F, Liu Z, Wan Y, Shi Z. Finite element simulation of machining of Ti-6Al-4V alloy with thermodynamical constitutive equation. The International Journal of Advanced Manufacturing Technology 2010; 49: 431-439, https://doi.org/10.1007/s00170-009-2423-y.
36. Shrot A, Bäker M. Determination of Johnson-Cook parameters from machining simulations. Computational Materials Science 2012; 52 (1): 298-304, https://doi.org/10.1016/j.commatsci.2011.07.035.
37. Su C, Chen H, Wen Z. Prediction of remaining useful life for lithium-ion battery with multiple health indicators. Eksploatacja i Niezawodnosc - Maintenance and Reliability 2021; 23(1): 176-183, 10.17531/ein.2021.1.18.
38. Sun HB, Zhang JD, Mo R, Zhang XZ. In-process tool condition forecasting based on a deep learning method. Robotics and Computer-Integrated Manufacturing 2020; 64: 101924, https://doi.org/10.1016/j.rcim. 2019.101924.
39. Tamizharasan T, Kumar S. Optimization of cutting insert geometry using DEFORM-3 D: numerical simulation and experimental validation. International Journal of Simulation Modelling 2012; 11(2): 65-76, https://doi.org/10.2507/IJSIMM11(2)1.200.
40. Wang Y, Su HH, Dai JB, Yang SB. A novel finite element method for the wear analysis of cemented carbide tool during high speed cutting Ti6Al4V process. The International Journal of Advanced Manufacturing Technology 2019; 103, 2795-2807, https://doi.org/10.1007/s00170-019-03776-1.
41. Wu DZ, Jennings C, Terpenny J, Gao RX, Kumara S. A comparative study on machine learning algorithms for smart manufacturing: tool wear prediction using random forests. Journal of Manufacturing Science and Engineering-Transactions of the ASME 2017; 139(7): 071018, https://doi.org/10.1115/ 1.4036350.
42. Xiang JW, Zhong YT. A novel personalized diagnosis methodology using numerical simulation and an intelligent method to detect faults in a shaft. Applied Sciences 2016; 6(12) 414, https://doi.org/10.3390/ app6120414.
43. Xu Z, Guo D, Wang J, Ge D. A numerical simulation method for a repairable dynamic fault tree. Eksploatacja i Niezawodnosc - Maintenance and Reliability 2021; 23(1):34-41, https://doi.org/10.17531/ein.2021.1.4.
44. Zhou J, Pang C, Zhong Z, Lewis F. Tool wear monitoring using acoustic emissions by dominant- feature identification. IEEE Transactions on Instrumentation and Measurement 2011; 60(2): 547-559, https://doi.org/10.1109/TIM.2010.2050974.
45. Zhou YQ, Sun BT, Sun WF. A tool condition monitoring method based on two-layer angle kernel extreme learning machine and binary differential evolution for milling. Measurement 2020; 16(15): 186-196, https://doi.org/10.1016/j.measurement.2020.108186.
46. Zhou YQ, Sun BT, Sun WF, Lei Z. Tool Wear Condition Monitoring Based on a Two-layer Angle Kernel Extreme Learning Machine using Sound Sensor for Milling Process. Journal of Intelligent Manufacturing 2020; 9, https://doi.org/ 10.1007/s10845-020-01663-1.
47. Zhou YQ, Sun WF. Tool Wear Condition Monitoring in Milling Process Based on Current Sensors. IEEE Access 2020; 8: 95491-95502, https://doi.org/10.1109/ACCESS.2020.2995586.
48. Zhou YQ, Xue W. A multisensor fusion method for tool condition monitoring in milling. Sensors 2018; 18(11): 3866, https://doi.org/10.3390/s18113866.
49. Zhou YQ, Xue W. Review of tool condition monitoring methods in milling processes. The International Journal of Advanced Manufacturing Technology 2018; 96(3-4): 2509-2523, https://doi.org/10.1007/s00170- 018-1768-5.
50. Zhu KP, Liu T. Online tool wear monitoring via hidden semi-Markov model with dependent durations. IEEE Transactions on Industrial Informatics 2018; 14(1): 69-78, https://doi.org/10.1109/TII.2017.2723943.